

“© 2022 IEEE. Personal use of this material is permitted. Permission from IEEE must be obtained for all other uses, in any current or future media, including reprinting/republishing this material for advertising or promotional purposes, creating new collective works, for resale or redistribution to servers or lists, or reuse of any copyrighted component of this work in other works.”

Intra-Body Molecular Communication via Blood-Tissue Barrier for Internet of Bio-Nano Things

Muneer M. Al-Zubi¹, Ananda S. Mohan², Peter Plapper³, and Sai Ho Ling²

Abstract—Molecular communication is an emerging communication paradigm that allows bio-nanomachines to communicate using biochemical molecules as information carriers. It can be used in many promising biomedical applications such as the Internet of Bio-Nano Things (IoBNT) for targeted drug delivery and healthcare applications. In particular, the blood-tissue barrier inside the body forms the main communication pathway for molecular information exchange between the nanomachines as well as between the intra-body nanonetwork and the Bio-Cyber interface in the IoBNT network. However, overcoming this barrier by the molecules is one of the main challenges for molecular communication in the body. Therefore, spatiotemporal modeling of molecular communication across the blood-tissue barrier is of particular interest. In this paper, we develop a mathematical model and stochastic particle-based simulator for molecular communication over high spatiotemporal resolution between **mobile** bio-nanomachines in the blood capillary and the surrounding tissue. The transmitting bio-nanomachine is modeled as a **moving** sphere with a continuous emission pattern over a specific duration. In this work, the blood capillary characteristics including the blood-tissue barrier and blood flow are modelled and their effect is examined on the molecular received signal. In addition, we examined the impact of the emission duration, the elimination rate, and the separation distance on the molecular received signal. The numerical results are verified using the developed particle-based simulator. This work can help in the optimum design and development of the IoBNT systems based on molecular communication for biomedical applications such as smart drug delivery and health monitoring systems.

Index Terms—Bio-cyber interface, bio-nano things, blood-tissue barrier, molecular communication, nanomachine, nanonetwork.

I. INTRODUCTION

The recent advances in bio-nanotechnology help in designing synthetic nanoscale computing and actuation devices (aka, nanomachines, nanorobots, or Bio-Nano Things), that contain tiny components usually made of either biological or bio-compatible materials [1]. The bio-nanomachines (NMs) are small devices that have sizes ranging from a macromolecule size to biological cell size. These NMs can perform simple tasks such as computation, actuation, and sensing. The researchers aim to make these NMs capable of performing more complex tasks

such as targeted drug delivery, health monitoring, cancer detection, etc [2, 3]. This goal can be achieved through communications and mutual coordination between a group of NMs in a nanonetwork.

Molecular communication (MC) has a great potential to implement the communication between the NMs inside the body, i.e., Intra-body nanonetwork, to provide advanced medical applications such as targeted drug delivery and disease detection [4]. Molecular communication is a communication mechanism that is biologically inspired by cellular communication via biochemical molecules between the cells inside the body [5, 6]. In recent years, MC has received great attention from several researchers around the world. Compared to wireless communication using electromagnetic (EM) waves, MC is a more realistic and efficient communication technique between NMs inside the body due to its powerful features such as biocompatibility, low energy requirements, small size, and it is not subject to the requirements of antenna size and frequency [7, 8]. The capability of nanorobots to perform controlled tasks, e.g., drug release, has been established at a laboratory scale, e.g., DNA-based nanorobots [2].

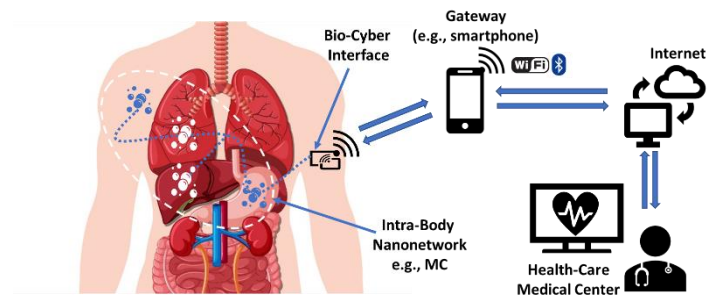


Fig. 1. Typical Internet of Bio-Nano Things (IoBNT) Architecture.

A group of bio-nanomachines, moving in the blood and the surrounding tissues, forms the intra-body nanonetwork where they communicate collaboratively to perform specific tasks such as sensing the biological and chemical changes in the human body. In addition, the intra-body nanonetworks can be used to perform medical actuation based on commands sent remotely from an external device. In the future, it is expected

Muneer M. Al-Zubi was with the University of Technology Sydney (UTS), Sydney, Australia. He is now with the Department of Engineering, University of Luxembourg, Luxembourg, Luxembourg (e-mail: muneer.al-zubi@uni.lu; muneermaz85@gmail.com).

Ananda S. Mohan was with the Centre for Health Technologies, University of Technology Sydney (UTS), Sydney, Australia (e-mail: anandasaganavarapu@gmail.com).

Peter Plapper is with the Department of Engineering, University of Luxembourg, Luxembourg, Luxembourg (e-mail: peter.plapper@uni.lu).

Sai Ho Ling is with the School of Electrical and Data Engineering, University of Technology Sydney (UTS), Sydney, Australia (e-mail: steve.ling@uts.edu.au).

> REPLACE THIS LINE WITH YOUR MANUSCRIPT ID NUMBER (DOUBLE-CLICK HERE TO EDIT) <

that MC will provide the communication capability between the NMs to perform different complex sensing and actuation tasks cooperatively. The communicating NMs through Intra-body nanonetwork can be further connected to an external network (e.g., the internet) via a Bio-Cyber interface to extend their capability and efficiency to support more complex real-world biomedical applications. The Bio-Cyber interface is used to convert molecular signals of the intra-body nanonetworks into an electrical signal for the cyber domain of the Internet (and vice versa) [9, 10]. Thus, the communication between the NMs and the external internet network via the Bio-Cyber interface will form the Internet of Bio-Nano Things (IoBNT) framework as shown in Fig. 1. The IoBNT can enable the NMs inside the body to send the collected biosensor data over the Internet to an external monitoring device for further processing. Moreover, the NMs can receive an external command remotely to perform a specific task such as medical actuation and drug release. In this scenario, the bio-cyber interface is assumed to be capable to communicate with a nearby gateway device (e.g., a smartphone) over relatively short distances using low-power communication technology such as Bluetooth Low Energy (BLE) or Radio Frequency Identification (RFID) [9]. Then, the smartphone can send and receive the data through a remote access point connected to the internet network. Alternatively, the bio-cyber interface could be designed to present the biochemical information as a visualized output via flexible skin-attachable displays, e.g., light-emitting diodes and capacitors [11]. Then, the obtained visual information can be read out using a smartphone before sending it to the internet network via the remote access point.

In the Intra-body nanonetworks, the bio-nanomachines enter the body through injection into the blood and then navigate autonomously throughout the body to reach the blood capillary network. The capillary is a tiny blood microvessel with a diameter in a micrometer scale and has a very thin wall of endothelial cells i.e., the endothelium layer. This layer forms the blood-tissue barrier (BTB) that hinders the transport of certain molecules between blood and the surrounding tissue, e.g., the blood-brain barrier (BBB) [12]. This barrier represents the main MC pathway for molecular transport between NMs as well as between the intra-body nanonetwork and the bio-cyber interface in the IoBNT network. Thus, overcoming this biological barrier is one of the main challenges for MC between nanomachines. In this scenario, mobile NMs located inside the blood communicate with other NMs or bio-cyber interfaces in the surrounding tissue across the BTB. The MC channel through which information molecules are transported and interacted between blood capillary and the surrounding tissue across the BTB has a significant impact on the molecular signals received by the NMs and bio-cyber interface. Thus, modelling of MC in such complex biological propagation channel over high spatial-temporal nanoscale for different transmitted molecular patterns is of particular interest for optimum design and development of the IoBNT infrastructure including bio-nanomachines and Bio-Cyber interfaces. Mathematical and stochastic modelling of MC provides a clear understanding of molecule transport and interaction over a wide range of spatial-temporal scales in a flexible and

comprehensive manner. Moreover, it plays an essential role in reducing the number of experiments to save time and cost.

Molecular communication enables promising medical applications inside the body, particularly through the blood vessels and capillaries. In [13], a blood viscosity monitoring system is proposed using MC by simulating the molecular received signal through a set of receptors located on the inner surface of a blood vessel. In [14], the authors proposed a flow-based MC model to detect the deformability of the red blood cells based on measuring the nanoparticle concentration inside blood vessels. Abnormality detection inside the blood vessels is modelled using multiple cooperative nanomachines in [15]. A simulation-based MC system is developed for the detection and monitoring of inflammatory levels of COVID-19 disease in the blood vessels [16]. In [17, 18], targeted drug delivery systems are developed based on the MC paradigm by modelling the drug transport through the blood vessels and capillary network. In addition, other MC models had been addressed from the perspective of data communication inside cylindrical vessel-like channels. In [19], an underlay cognitive MC model is developed inside a cylindrical channel with anomalous diffusion. The performance of MC systems inside vessel-like channels with drift has been evaluated in terms of bit error rate, achievable data rates, inter-symbol interference, etc, e.g., [20-23]. In [24], we proposed a biosensing platform, attached to a vascular stent, for the detection of atherosclerotic biomarkers inside the artery. In [25], the authors developed a two-compartment model for IoBNT architecture including the MC between the bio-cyber interface and the nanonetwork. However, the classic compartmental approach is limited to studying the volume averaging of molecules distribution over large temporal scales under the assumption that the molecules are homogeneously distributed in the compartments. Therefore, this approach is inappropriate for modelling the MC systems where the molecular distribution and the physicochemical interactions are highly varied over a very small spatiotemporal scale depending on the locations of the NMs and the emission patterns. This can also be seen from our results in this paper. However, none of the works in the literature considered studying the MC across the BTB between the NMs or between the nanonetwork and the bio-cyber interface over high spatiotemporal resolution. In addition, no stochastic particle-based simulator has been proposed for this system in the literature.

In this paper, we develop a mathematical model and stochastic particle-based simulator over high spatial-temporal resolution for MC between mobile bio-nanomachines, located in the blood capillary and the surrounding tissues. The developed models can also be used for modeling the MC between the NMs and the Bio-Cyber interface in IoBNT infrastructure. The proposed work provides important insights in modelling the intra-body nanonetworks in which the mobile NMs, within the capillaries, communicate with the surrounding bio-cyber interface and other NMs across the BTB. In this work, we obtain the molecular received signal by the NMs considering the impact of the BTB. The emission process of

> REPLACE THIS LINE WITH YOUR MANUSCRIPT ID NUMBER (DOUBLE-CLICK HERE TO EDIT) <

transmitting nanomachine (TN) is modelled using a continuous emission pulse. It is important to understand how the blood, tissue, and BTB affect the distribution and interaction of the molecules to accurately predict the molecular received signal by the NMs or the Bio-Cyber interface. To the best of our knowledge, this is the first work in the literature that addresses the MC between NMs across the BTB over a high spatial-temporal resolution to characterize the MC channels and molecular received signal.

This paper is organized as follows. Firstly, we introduce the proposed system and the mathematical formulation in section II. The particle-based simulation framework is presented in section III. In section IV, the numerical and simulation results are discussed. Finally, the paper is concluded in section V.

II. SYSTEM MODEL

In this system, a spherical TN, located inside the blood capillary, communicates across the BTB with another nanomachine (NM) or Bio-Cyber interface in the surrounding tissue as a part of the IoBNT network, see Fig. 2. After injection of the NMs into the blood, they navigate autonomously to reach the target capillary. Then, the TN will enter the capillary at the initial position $w_0 = (x_0, y_0, z_0)$, and then it moves with the blood flow inside the capillary. In this work, the initial position is chosen at the capillary inlet, i.e., the origin point (0,0,0).

The TN is assumed to be loaded with a specific amount of information molecules and it can release the molecules in response to an external stimulus, e.g., magnetic field, ultrasound, etc. Here, we assume that the external trigger (stimulus) is applied to the target capillary for a specific duration after the TN enters the capillary. Thus, this will allow the TN to release the molecules continuously over an emission duration (T_{on}). After that, the remaining amount of molecules inside the TN will depend on the emission duration and the initially loaded molecules.

In the real world, the emission process takes a period of time even for the ideal impulsive release which can be obtained by choosing a very short emission period. The continuous release pattern over a specific duration is a more general emission profile that is suitable for various modulation techniques such as M -ary concentration shift keying (CSK). Moreover, this emission pattern is suitable for targeted drug delivery applications where a specific amount of drug is required to be delivered by the NMs to the target location over a specific period. The emitted molecules diffuse independently in all directions (3-D diffusion) following random Brownian motion and they are also driven by the blood flow along the axial direction. Finally, a portion of the emitted molecules will reach the receiver in the tissue surrounding the blood capillary. In this paper, the receiver represents either a receiving nanomachine (RN) or a bio-cyber interface. The receiver is a passive sphere that is assumed to have the capability of counting the molecules without either impeding the diffusion or creating any reactions. The biological environment (i.e., the propagation channel) is assumed to be composed of two regions, namely, blood and tissue, separated by the BTB (i.e., a semipermeable interface

consisting of endothelial cells). The blood and tissue regions have distinct diffusivities and thicknesses. A portion of the transmitted molecules can move across this barrier and therefore it is modelled as a semipermeable layer with a permeability coefficient (P_m). Compared to the larger blood vessels such as arteries, the velocity of blood flow is very small in the capillaries which provides enough time for molecules (e.g., gases and nutrients) to exchange between blood and the tissue. The blood velocity may vary due to changes in blood pressure, vessel resistance, blood viscosity, etc. Here, we assume the velocity of blood flow is uniform with velocity v in the axial direction and is equal to the average velocity of the Poiseuille model over the radial direction [15, 20].

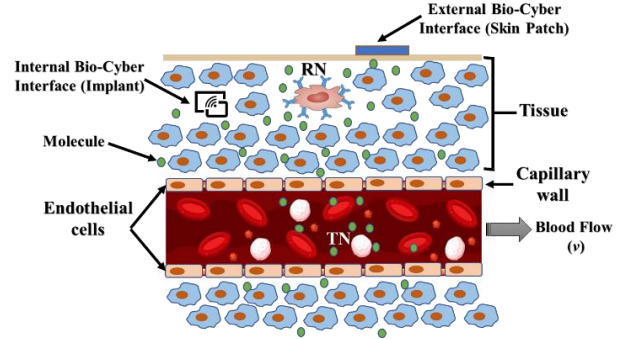


Fig. 2. Graphical representation of MC between NMs in the blood capillary and the surrounding tissue across the BTB.

The molecular transport is driven by both advection (i.e., flow) and diffusion (i.e., Brownian motion). Thus, the transport of information molecules is mathematically described using the following advection-diffusion equation [19].

$$\frac{\partial C(w, t)}{\partial t} = D \nabla^2 C(w, t) - v \cdot \nabla C(w, t) - \gamma C(w, t) + S(w, t) \quad (1)$$

where C is the molecular concentration in (mol/m^3) at the position $w = (x, y, z)$ at time t , ∇^2 is the Laplacian operator, ∇ is the gradient operator, and D is the diffusion coefficient (diffusivity) of the medium in (m^2/s). The diffusivity is a physical constant that describes how fast the random movements of the molecules within the medium which depends on molecule size, temperature, and the medium viscosity. The parameter v is the blood flow velocity inside the capillary in (m/s) and γ is the apparent first-order elimination rate constant in (s^{-1}). This elimination constant accounts for the combined effect of the various physical and chemical reaction processes on the molecules such as clearance into the capillaries, binding or uptake to cells, or enzymatic degradation. This process is fundamental in pharmacokinetics and it is usually modelled using a first-order reaction mechanism [26]. The function $S(w, t)$ is the molecular source term as a function of time and location in the unit of $\text{mol}/(\text{s} \cdot \text{m}^3)$.

The blood capillary can be considered as a cylindrical tube; thus, we will transform the advection-diffusion equation to the cylindrical coordinate system. Thus, assuming the diffusion to be symmetrical around the capillary axis (z -axis), (1) can be

> REPLACE THIS LINE WITH YOUR MANUSCRIPT ID NUMBER (DOUBLE-CLICK HERE TO EDIT) <

expressed for the blood and the surrounding tissue regions as

$$\frac{\partial C_b(r, z, t)}{\partial t} = D_b \left[\frac{\partial^2 C_b(r, z, t)}{\partial r^2} + \frac{1}{r} \frac{\partial C_b(r, z, t)}{\partial r} + \frac{\partial^2 C_b(r, z, t)}{\partial z^2} \right] - v \cdot \nabla C_b(r, z, t) - \gamma_b C_b(r, z, t) + S(r, z, t) \quad (2)$$

$$\frac{\partial C_t(r, z, t)}{\partial t} = D_t \left[\frac{\partial^2 C_t(r, z, t)}{\partial r^2} + \frac{1}{r} \frac{\partial C_t(r, z, t)}{\partial r} + \frac{\partial^2 C_t(r, z, t)}{\partial z^2} \right] - \gamma_t C_t(r, z, t) \quad (3)$$

Here, $C_b(r, z, t)$ and $C_t(r, z, t)$ represent the concentration of the molecules at the radial position r and the axial location z in blood and tissue, respectively. The parameters (D_b , D_t) and (γ_b , γ_t) are the diffusivities and effective elimination constants in blood and tissue, respectively. The radial distance from the capillary axis is given as $r = \sqrt{x^2 + y^2}$. Here, the molecular transport in the extracellular space of the surrounding tissue is assumed to be dominated by diffusion rather than bulk flow [27, 28]. The source term $S(r, z, t)$ appears only in (2), i.e., the blood region, because the TN is located inside the capillary.

We assume the concentration of the information molecules is uniformly distributed over the entire volume of the TN. In addition, we assumed that the external stimulus is applied to the target region when the TN enters the capillary and thus it starts releasing the molecules immediately.

In order to make the model flexible and suitable for different emission rate profiles, we have modelled the emission process in the TN as a continuous pulse over a period (T_{on}). The emission duration is controlled via varying the duration of the applied external stimulus, e.g., magnetic field, ultrasound, etc. Thus, the source term can be expressed as

$$S(t) = M_0 \times \text{rect} \left(\frac{t - T_{on}/2}{T_{on}} \right) \times \delta(z - vt - z_0) \delta(r - r_0) \quad (4)$$

where M_0 is the emission rate in (mol/s.m^3), $\text{rect}(\cdot)$ is the rectangular function, and $\delta(\cdot)$ is the Dirac delta function.

Here, TN will move in the direction of the z -axis inside the capillary at the same speed as the blood flow. Thus, the effective flow velocity and the relative motion between the released molecules and the mobile TN are negligible [15, 23]. To simplify the mathematical analysis and simulation process, we assume that the TN does not change its location in the radial direction and its movement is along the z -axis. Therefore, in this work, it is assumed that the impact of the TN motion on the release process is negligible and the TN does not collide with the blood cells.

Zero flux boundary condition is applied at the outer surface of the tissue as

$$-D_t \nabla C_t(r, z, t) = 0, \quad r = r_t \quad (5)$$

where r_t is the radius of the tissue region.

The BTB consists of a single endothelial cell layer that lines the blood capillaries and regulates the exchange of molecules between the bloodstream and the surrounding tissues [12]. The information molecules can diffuse through the pores between the endothelial cells of the capillary wall as well as through the cell membranes as shown in Fig. 3. Here, we ignore active transport across the capillary wall. There is a concentration gradient at the capillary wall due to the concentration difference on both surfaces which creates a diffusional flux from the region of high concentration to the region of low concentration.

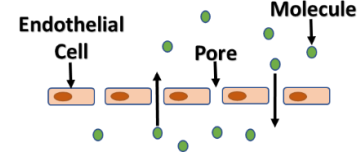


Fig. 3. Transport of the molecules via the endothelial layer.

The interface between blood and tissue, i.e., the capillary wall, can be considered as a thin semipermeable barrier with an effective permeability $P_m = D_m/L_m$, where L_m and D_m are the thickness and effective diffusivity of the barrier. The flux boundary conditions on each side of the barrier are defined as

$$D_b \nabla C_b(r, z, t) = P_m (C_b(r, z, t) - C_t(r, z, t)) \quad (6)$$

$$D_t \nabla C_t(r, z, t) = P_m (C_t(r, z, t) - C_b(r, z, t)) \quad (7)$$

where P_m is the effective permeability of the endothelial layer in (m/s). It determines the ability of the molecules to pass and diffuse through the endothelial layer [28]. As the permeability increases, the interface becomes more permeable which makes the molecules more likely to cross the layer to the surrounding regions. The permeability depends on the intrinsic permeability of the layer and the molecular characteristics such as the size and shape of the molecules which are included in the diffusion coefficient. Moreover, the permeability may be affected due to inflammation or damage of the capillary [28]. Here, the boundary conditions which are given by (6)-(7), allow for possible changes in the concentration at the barrier in relation to the permeability coefficients.

In addition, it is assumed that the red blood cells move at the same velocity as the fluid medium (i.e., the bloodstream). Moreover, the impact of the red blood cells on the propagation of the molecules can be included via the apparent combined effect of the blood diffusion coefficient (or viscosity), blood clearance/elimination rate, and blood flow velocity. Therefore, we assume that the impact of the movement of the blood cells on the diffusive molecules is negligible and it can be included in other system parameters.

The analytical solution of the molecular diffusion equations in a composite multilayer cylindrical environment is complicated and is not analytically tractable. In addition, the BTB interface between the blood and the tissue is semipermeable (i.e., with diffusion resistance) and thus it adds further complexity. Therefore, we have modelled and solved this system numerically using COMSOL Multiphysics® software which is based on the finite element method. The

> REPLACE THIS LINE WITH YOUR MANUSCRIPT ID NUMBER (DOUBLE-CLICK HERE TO EDIT) <

numerical results are validated using our developed stochastic particle-based simulator over high spatial-temporal resolution as will be described in the next section.

III. STOCHASTIC PARTICLE-BASED SIMULATION

Stochastic particle-based simulation provides a precise prediction for the molecular received signal by tracking the random position of each molecule individually within the simulation environment. In this section, we develop a comprehensive stochastic particle-based simulator for MC across the BTB between spherical NMs located inside the capillary and the surrounding tissue. Moreover, we build a stochastic simulation framework for the continuous emission of the information molecules from a spherical TN **moving** inside the blood capillary. The simulation is developed using MATLAB to validate the numerical results. The simulation time T is divided into several time steps with a time width Δt . The emission process from the TN, moving in the capillary **from an initial position** (x_0, y_0, z_0) , is modeled as a continuous pulse with emission period T_{on} . The number of emission time-steps N_E is equal to $T_{on}/\Delta t$. In each time step, a number of molecules equal to N_m/N_E are uniformly distributed inside the spherical TN as shown in Fig. 4.

The molecules move randomly in all directions under the effect of the diffusion, i.e., Brownian motion. Moreover, the movement of the molecules inside the capillary is derived by the blood flow along the axial direction, i.e., the z -axis. The locations of the information molecules are tracked and recorded at each time step. The random location of each molecule at the time instant $t=i\Delta t$ is updated as [29],

$$(x_i, y_i, z_i) = (x_{i-1}, y_{i-1}, z_{i-1}) + (\Delta x_i, \Delta y_i, \Delta z_i) \quad (8)$$

where $i=1, \dots, N_t$ and N_t is the number of time steps. The point $(x_{i-1}, y_{i-1}, z_{i-1})$ is the molecule location at the time $t=(i-1)\Delta t$, and $(\Delta x_i, \Delta y_i, \Delta z_i)$ is a random displacement over each spatial axis.

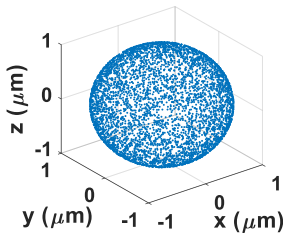


Fig. 4. The uniform distribution of molecules inside the spherical TN captured from the particle-based simulator.

The random displacement due to diffusion follows normal distribution $N(0, \sigma^2)$ with zero-mean and variance σ^2 equal to $(2D_b\Delta t)$ and $(2D_t\Delta t)$ in blood and tissue, respectively. However, along the axial axis, an additional displacement component $(v\Delta t)$ is added when the molecules move inside the blood capillary. When a molecule moves from the blood across the BTB to the surrounding tissue, it will be influenced by the diffusivity of the tissue and consequently, it will follow the mean-squared displacement in the tissue (and vice versa). The information molecule that reaches the **receiver** volume will be

counted and the counter increases by one at the end of the time step.

Moreover, the TN will move along the z -axis inside the capillary with a speed equal to the blood flow velocity according to the following equation:

$$Z_{TN,i} = Z_{TN,i-1} + v\Delta t \quad (9)$$

where $Z_{TN,i}$ is the current location of TN along the z -axis at the i^{th} time step and $Z_{TN,i-1}$ is its previous location at the $(i-1)^{\text{th}}$ time step.

Transport of the molecules across the BTB is stochastically modelled using the transmission probability. Some molecules will succeed in crossing the BTB and other molecules will be reflected into the capillary lumen, when hit the capillary boundary, depending on the transmission probability, given by [30] as

$$P_{rf} = \frac{k_f}{(k_f + k_b)^2} \left[2(k_f + k_b) - \sqrt{\frac{\pi}{2}} M(k) \right] \quad (10)$$

$$P_{rb} = P_{rf} (k_b/k_f) \quad (11)$$

where,

$$M(k) = 1 - e^{2(k_f+k_b)^2} \operatorname{erfc}(\sqrt{2}(k_f + k_b)) \quad (12)$$

$$k_f = P_m \sqrt{\Delta t / 2D_b} \quad (13)$$

$$k_b = P_m \sqrt{\Delta t / 2D_t} \quad (14)$$

where k_f and k_b are the dimensionless permeability coefficients of the BTB in the forward and backward directions, respectively.

The location of molecules is checked at the end of each time step and the molecules that hit the capillary wall will be assigned with uniformly distributed random numbers having values between zero and one. If the transmission probability P_r is larger than the random number, then the molecule will transport across the wall from the blood to the surrounding tissue if the molecule was in the blood or from the tissue to the blood if the molecule was in the tissue. Otherwise, the molecule will be reflected back to its previous position.

The molecular degradation in the environment is modelled using a first-order degradation reaction. At each time step, a uniformly distributed random number with a value between zero and one is assigned for each molecule. If the degradation probability, given by (15) [26], is greater than the random number then the molecule will be eliminated from the simulation environment.

$$P_{rd} = 1 - e^{-\gamma\Delta t} \quad (15)$$

The molecular received signal represents the concentration of the molecules inside the **receiver** volume over time. Assuming the **receiver** is sufficiently far from the TN, the concentration inside the **receiver** volume can be considered uniform. Thus, the concentration is evaluated by dividing the total number of

> REPLACE THIS LINE WITH YOUR MANUSCRIPT ID NUMBER (DOUBLE-CLICK HERE TO EDIT) <

received molecules at each time-step $\bar{N}(\Delta t)$ over the receiver volume (V_{rx}). Then, we obtain the molecular received signal by normalizing the concentration to the total number of released molecules (N_m) as follows

$$M(\Delta t) = T_{on} V_{tx} \frac{\bar{N}(\Delta t)}{N_m V_{rx}} \quad (16)$$

Equation (16) is multiplied by the term ($T_{on} V_{tx}$) to convert the molecular emission rate M_o , to the number of emitted molecules in the simulator.

IV. NUMERICAL AND SIMULATION RESULTS

In this work, the MC channel between the NMs consists of a 3-D cylindrical capillary and the surrounding tissue, separated by the BTB. The mathematical model is numerically solved using COMSOL Multiphysics® software. A time-dependent solver is used to solve the advection-diffusion equations with the boundary conditions and the source term. **The TN is defined as a spherical object using a variable expression that depends on both the time and velocity that determines the strength and current location of the TN inside the geometry.** The mesh size used to discretize the geometry is chosen as finer mesh based on an independent mesh test which shows a negligible improvement on the molecular received profile for an extra reduction in the mesh size. In addition, we refine the mesh at the interfaces between the blood and the surrounding tissue as well as between the TN volume and the surrounding blood region. This mesh refinement is applied at these interfaces to handle the rapid change in the molecular concentration. The numerical results are compared and verified with the stochastic particle-based simulation.

The common system parameters used in our analysis are listed in Table 1 (unless stated otherwise) with values chosen based on the published works in the literature [28, 29]. However, these parameters may have different values depending on the characteristics of both the molecules and the environments in which the molecules diffuse. The TN may have a range of sizes that fit within the capillary lumen. For example, Liposome nanocarriers and the nanorobots have a range of sizes as 0.025-2.5 μ m and 0.1-10 μ m, respectively. Thus, the radius of the TN is chosen within a realistic range, i.e., 1 μ m. Moreover, these NCs can be designed with various emission durations that may range from milliseconds to seconds. Thus, we examine the model for a range of emission duration between 0.1 to 1s. The radius of the small capillary in the human body normally ranges between 3-5 μ m, thus we chose the radius equal to 5 μ m. The permeability is chosen within a reasonable range given by [28], i.e., 6 $\times 10^{-8}$ -1 μ m/s. The diffusivities of blood and tissue are selected according to [28, 29]. For example, the diffusivity in brain tissue may range between 10-1500 μ m²/s. The elimination rate is chosen according to the experimental range found in the literature, i.e., 1.1 $\times 10^{-4}$ -6.8 $\times 10^7$ s⁻¹, see [28]. The simulation parameters, e.g., the time-step and the number of released molecules, are chosen by performing a trial and error run with different values to examine the variations in the output received signal. We found that a time-step with values less than 0.1ms, will not lead to significant variation in the simulation results.

In this work, the receiver is located at position ($x, y, 500$) μ m where the coordinates (x, y) determine the radial position from the capillary axis (z -axis). In this paper, all simulation results are obtained by averaging over 300 independent realizations. Here, the terms molecular concentration profile and molecular received signal are used interchangeably. Moreover, the following terms are used to refer to the BTB: the capillary wall, the barrier, and the endothelial layer.

TABLE I
MODEL PARAMETERS (UNLESS STATED OTHERWISE) [28, 29]

Parameter	Value	Unit	Description
P	5×10^{-7}	m/s	Permeability of capillary wall
L_m	2	μ m	Thickness of capillary wall
D_m	1	μ m ² /s	Diffusivity of capillary wall
L_c	1	mm	Capillary Length
r_b	5	μ m	Capillary radius
v	100	μ m/s	Velocity of blood flow
D_b	37	μ m ² /s	Diffusivity of blood
D_t	131	μ m ² /s	Diffusivity of tissue
γ_b	0	1/s	Elimination rate in blood
γ_t	0	1/s	Elimination rate in tissue
r_t	250	μ m	Radial thickness of tissue
r_{tx}	1	μ m	Transmitter radius
T_{on}	500	ms	Emission duration
(x_0, y_0, z_0)	(0,0,0)	μ m	Transmitter Location
(x, y, z)	(0,50,500)	μ m	Receiver Location
M_o	1	mol/s.m ³	Emission rate
Δt	0.1	ms	Simulation Step time
N_m	10^4	-	Number of emitted molecules
-	300	-	Iterations number

Figure 5 shows the molecular received signal as a function of time for different emission periods at the TN. The numerical results match very well with the stochastic results obtained from the particle-based simulator. Indeed, when the emission duration is extended, the received signal shows a higher amplitude. This happens because the amount of the emitted molecules increases with extending the emission time and thus the number of the molecules that reach the **receiver** will increase. An approximation for the channel impulse response can be obtained when the emission time is made equal to a very short duration, i.e., impulse function. **The peak amplitude shows an increase approximately by a factor of 4 when $T_{on} = 0.5$ s and by a factor of 8 when $T_{on} = 1$ s.** The impact of the emission period on the peak time is not noticeable for this case, but there is an increase in the peak time for the longer emission periods. This happens because new molecules will continue visiting the receiver for a longer period as the emission period

> REPLACE THIS LINE WITH YOUR MANUSCRIPT ID NUMBER (DOUBLE-CLICK HERE TO EDIT) <

increases. Moreover, we can observe that the received signal shows zero value in the first few seconds (~6s) because the molecules require time to reach the receiver which is relatively located far from the TN.

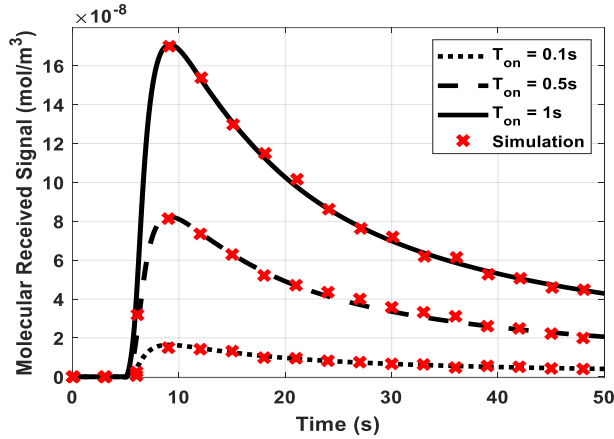


Fig. 5. Temporal molecular received signal for various emission durations.

The molecular received signal versus the separation distance between the capillary and the receiver is plotted for various elimination rate constants in Fig. 6. We can observe a significant reduction in the received signal (i.e., distribution of the molecules) as the receiver is located far away from the capillary and the TN. This happens because the probability of visiting the receiver by the molecules becomes lower with increasing the separation distance between the NMs. Moreover, the molecular received signal is affected by the elimination rate which is modelled as a first-order reaction process. The larger elimination rate constant leads to a smaller concentration level at the receiver and vice versa. This could happen due to an increase in both the number of degraded molecules which will not be recognized by the receiver thereafter and the number of eliminated molecules that will not reach the receiver. As an example, when the receiver is located at a distance of 50 μm , an increase in the elimination rate to $1 \times 10^{-2} \text{ s}^{-1}$ and $5 \times 10^{-2} \text{ s}^{-1}$ leads to a decrease in the signal amplitude by a factor of 1.2 and 2.75, respectively. However, as the separation between the NMs increases, the impact of the elimination rate constant on the molecular received signal decreases, i.e., all the curves converge for various elimination rate constants. This could be because the separation distance becomes the dominant factor on the concentration profile instead of the elimination rate where the number of molecules that reach the receiver will be very low at a very far location.

The permeability of the blood capillary wall (i.e., the BTB) has a direct influence on the molecular received signal by the receiver which is located outside the capillary, i.e., in the surrounding tissue, as shown in Fig. 7. This permeability depends on the effective diffusivity and thickness of the capillary wall. As the capillary wall (barrier) becomes more permeable for the molecules, the number of molecules that can pass through the barrier to the surrounding tissue increases. Thus, the molecular received signal at the receiver will increase.

Accordingly, a larger number of molecules can visit the receiver within a shorter time which leads to a decrease in the signal peak time. We can observe that the peak amplitude increases by a factor of 3 and 4 when P_m increases from 0.04 $\mu\text{m/s}$ to 0.2 $\mu\text{m/s}$ and 1 $\mu\text{m/s}$, respectively.

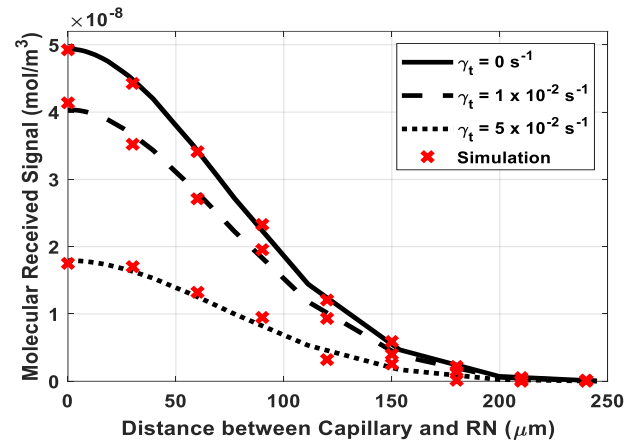


Fig. 6. The molecular received signal versus the separation distance for various elimination rate constants, taken at $t = 25\text{s}$.

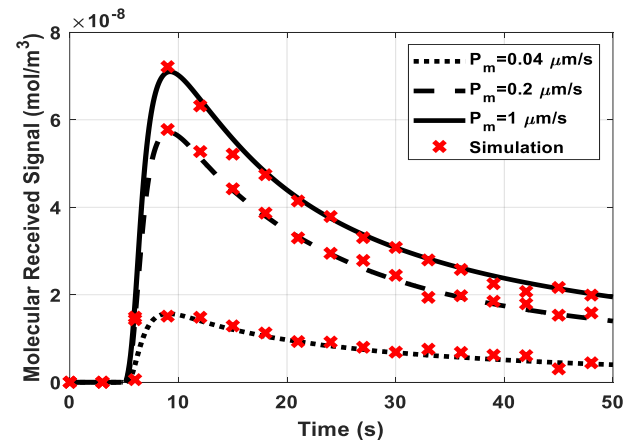


Fig. 7. The molecular received signal as a function of time for various permeability coefficients of the BTB.

The color map of the spatiotemporal distribution of the information molecules in the tissue, surrounding the blood capillary, is shown in Fig. 8. After emitting the molecules from the TN, which is moving inside the blood capillary, the molecules will diffuse to the surrounding tissue across the BTB. As expected, the molecular concentration decreases as the radial distance between the receiver and the capillary increases with the highest concentration achieved when the receiver is located near the capillary. Moreover, we can observe the movements of the molecules in the axial direction with time due to the effect of blood flow. Thus, the emitted molecules will continue moving inside the capillary via the blood flow along the axial direction and at the same time diffuse across the capillary wall in the radial direction. Finally, the molecules will be eliminated from the blood and the tissue as shown in Fig. 8 at $t=50\text{s}$ as they will move to other parts of the body and/or be removed by the various physicochemical processes as

demonstrated before. In addition, the transport and distribution of the molecules will be affected by the movement of the TN inside the capillary. However, if the emission duration is very short, the TN will release the molecules very fast within the first few micrometers. Thus, the TN movement after that will not have an impact on the molecule distribution. For example, if the TN moves in a blood flow with a velocity of $100\mu\text{m/s}$, it will stop releasing the molecules at a distance of $10\mu\text{m}$ assuming the emission duration is 0.1s.

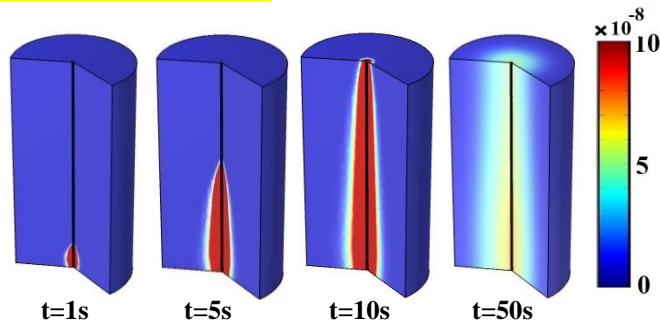


Fig. 8. Color map of the spatiotemporal molecular distribution taken at different instants in the tissue surrounding the capillary (i.e., the vertical centerline).

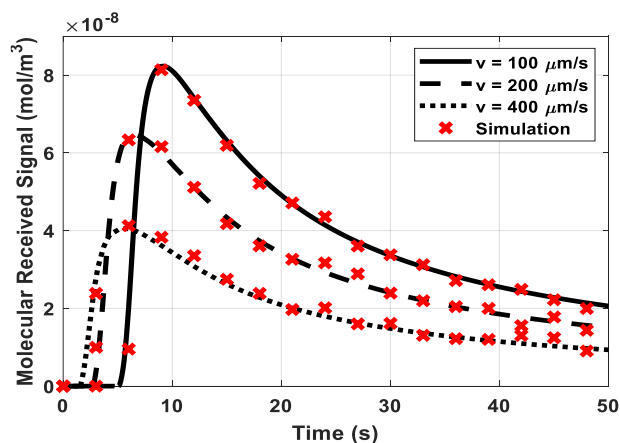


Fig. 9. Temporal molecular received signal for different blood flow velocities.

The temporal molecular received signal for various velocities of the blood flow is plotted in Fig. 9. The blood flow has a significant impact on the molecular signal received by the receiver which is located in the surrounding tissue. We can observe that the molecular received signal decreases as the velocity of blood flow increases. In this case, this happens because the molecules will move away faster from the receiver location as the blood velocity increases and thus fewer molecules will visit the receiver. When the flow velocity increases from $100\mu\text{m/s}$ to $200\mu\text{m/s}$ and $400\mu\text{m/s}$, the peak amplitude will be reduced by 25% and 50%, respectively. However, for other scenarios, the reverse may be true depending on the location of the NMs and the direction of the flow. Therefore, it is important to choose the right time and location to start emitting the information molecules by the NMs inside the blood capillary to achieve a stronger received signal by the receiver. Moreover, this figure shows the impact of the

blood velocity on the peak time of the received signal. An increase in the blood velocity leads to a reduction in the peak time because the molecules will reach faster the receiver.

V. CONCLUSION

In this paper, we propose a molecular communication system between mobile bio-nanomachines located in the blood capillary and the surrounded tissue across the BTB. The spherical TN releases the information molecules continuously over a period of time, i.e., the emission period. We developed a mathematical model and stochastic particle-based simulator for the proposed system. The molecules are exchanged across the wall of the blood capillary which is modelled as a thin semipermeable membrane. In this work, we examine the impact of various parameters on the molecular received signal at the receiver. The results show a significant impact for the blood capillary wall, the blood flow, the elimination rate, the emission duration, and the separation distance between TN and the receiver, on the molecular received signal. The molecular received signal shows higher amplitude when the emission duration and the capillary permeability are increased (and vice versa). However, the received signal is inversely proportional to both the blood flow velocity and the separation distance between the bio-nanomachines. The BTB represents the main pathway for MC molecular either between NMs or between the intra-body nanonetworks and bio-cyber interfaces. Thus, the proposed system can help in designing and optimizing the IoBNT systems based on MC Intra-body nanonetworks for biomedical applications such as disease detection, health monitoring, and targeted drug delivery.

REFERENCES

- [1] T. Nakano, A. W. Eckford, and T. Haraguchi, *Molecular communication*. Cambridge University Press, 2013.
- [2] S. Li *et al.*, "A DNA nanorobot functions as a cancer therapeutic in response to a molecular trigger in vivo," *Nature biotechnology*, vol. 36, no. 3, pp. 258-264, 2018.
- [3] L. Felicetti, M. Femminella, G. Reali, and P. Liò, "Applications of molecular communications to medicine: A survey," *Nano Communication Networks*, vol. 7, pp. 27-45, 2016.
- [4] Y. Tang, Y. Huang, C.-B. Chae, W. Duan, M. Wen, and L.-L. Yang, "Molecular type permutation shift keying in molecular MIMO communications for iobnt," *IEEE Internet of Things Journal*, 2021.
- [5] J. Wang, X. Liu, M. Peng, and M. Daneshmand, "Performance analysis of d-mosk modulation in mobile diffusive-drift molecular communications," *IEEE Internet of Things Journal*, vol. 7, no. 11, pp. 11318-11326, 2020.
- [6] H. Awan and C. T. Chou, "Improving the capacity of molecular communication using enzymatic reaction cycles," *IEEE transactions on nanobioscience*, vol. 16, no. 8, pp. 744-754, 2017.
- [7] J. Wang, M. Peng, Y. Liu, X. Liu, and M. Daneshmand, "Performance analysis of signal detection for amplify-and-forward relay in diffusion-based molecular communication systems," *IEEE Internet of Things Journal*, vol. 7, no. 2, pp. 1401-1412, 2019.
- [8] X. Chen, M. Wen, C.-B. Chae, L.-L. Yang, F. Ji, and K. K. Igorevich, "Resource Allocation for Multi-User Molecular Communication Systems Oriented to The Internet of Medical Things," *IEEE Internet of Things Journal*, 2021.
- [9] S. Zafar *et al.*, "A systematic review of bio-cyber interface technologies and security issues for internet of bio-nano things," *IEEE Access*, 2021.
- [10] I. F. Akyildiz, M. Pierobon, S. Balasubramaniam, and Y. Koucheryavy, "The internet of bio-nano things," *IEEE Communications Magazine*, vol. 53, no. 3, pp. 32-40, 2015.

> REPLACE THIS LINE WITH YOUR MANUSCRIPT ID NUMBER (DOUBLE-CLICK HERE TO EDIT) <

- [11] J. Y. Oh and Z. Bao, "Second skin enabled by advanced electronics," *Advanced Science*, vol. 6, no. 11, p. 1900186, 2019.
- [12] Q. Wen *et al.*, "Signaling pathways regulating blood–tissue barriers—Lesson from the testis," *Biochimica Et Biophysica Acta (BBA)-Biomembranes*, vol. 1860, no. 1, pp. 141-153, 2018.
- [13] L. Felicetti, M. Femminella, and G. Reali, "A molecular communications system for live detection of hyperviscosity syndrome," *IEEE transactions on nanobioscience*, vol. 19, no. 3, pp. 410-421, 2020.
- [14] Y. Sun, R. Z. Zhang, and Y. Chen, "A Molecular Communication Detection Method for the Deformability of Erythrocyte Membrane in Blood Vessels," *IEEE Transactions on NanoBioscience*, 2021.
- [15] N. Varshney, A. Patel, Y. Deng, W. Haselmayr, P. K. Varshney, and A. Nallanathan, "Abnormality detection inside blood vessels with mobile nanomachines," *IEEE Transactions on Molecular, Biological and Multi-Scale Communications*, vol. 4, no. 3, pp. 189-194, 2018.
- [16] L. Felicetti, M. Femminella, and G. Reali, "A molecular communications system for the detection of inflammatory levels related to COVID-19 disease," *IEEE Transactions on Molecular, Biological and Multi-Scale Communications*, 2021.
- [17] Y. Chahibi, M. Pierobon, S. O. Song, and I. F. Akyildiz, "A molecular communication system model for particulate drug delivery systems," *IEEE Transactions on biomedical engineering*, vol. 60, no. 12, pp. 3468-3483, 2013.
- [18] Y. Zhou and Y. Chen, "Latticed channel model of touchable communication over capillary microcirculation network," *IEEE transactions on nanobioscience*, vol. 18, no. 4, pp. 669-678, 2019.
- [19] S. Dhok, P. Peshwe, and P. K. Sharma, "Cognitive Molecular Communication in Cylindrical Anomalous-Diffusive Channel," *IEEE Transactions on Molecular, Biological and Multi-Scale Communications*, 2021.
- [20] N. Tavakkoli, P. Azmi, and N. Mokari, "Performance evaluation and optimal detection of relay-assisted diffusion-based molecular communication with drift," *IEEE transactions on nanobioscience*, vol. 16, no. 1, pp. 34-42, 2016.
- [21] N.-R. Kim, A. W. Eckford, and C.-B. Chae, "Symbol interval optimization for molecular communication with drift," *IEEE transactions on nanobioscience*, vol. 13, no. 3, pp. 223-229, 2014.
- [22] L. Chouhan, P. K. Sharma, and N. Varshney, "Optimal transmitted molecules and decision threshold for drift-induced diffusive molecular channel with mobile nanomachines," *IEEE transactions on nanobioscience*, vol. 18, no. 4, pp. 651-660, 2019.
- [23] N. Varshney, A. Patel, W. Haselmayr, A. K. Jagannatham, P. K. Varshney, and A. Nallanathan, "Impact of intermediate nanomachines in multiple cooperative nanomachine-assisted diffusion advection mobile molecular communication," *IEEE Transactions on Communications*, vol. 67, no. 7, pp. 4856-4871, 2019.
- [24] M. M. Al-Zu'bi and A. S. Mohan, "Implantable Biosensor Interface Platform for Monitoring of Atherosclerosis," *IEEE Sensors Letters*, vol. 4, no. 2, pp. 1-4, 2020.
- [25] U. A. Chude-Okonkwo, R. Malekian, and B. T. Maharaj, "Biologically inspired bio-cyber interface architecture and model for Internet of bio-nanotechnology applications," *IEEE Transactions on Communications*, vol. 64, no. 8, pp. 3444-3455, 2016.
- [26] M. M. Al-Zu'bi and A. S. Mohan, "Modeling of ligand-receptor protein interaction in biodegradable spherical bounded biological micro-environments," *IEEE Access*, vol. 6, pp. 25007-25018, 2018.
- [27] K. E. Holter *et al.*, "Interstitial solute transport in 3D reconstructed neuropil occurs by diffusion rather than bulk flow," *Proceedings of the National Academy of Sciences*, vol. 114, no. 37, pp. 9894-9899, 2017.
- [28] E. Vendel, V. Rottschäfer, and E. C. de Lange, "The need for mathematical modelling of spatial drug distribution within the brain," *Fluids and Barriers of the CNS*, vol. 16, no. 1, pp. 1-33, 2019.
- [29] M. M. Al-Zu'bi and A. M. Sanagavarapu, "Modeling a composite molecular communication channel," *IEEE Transactions on Communications*, vol. 66, no. 8, pp. 3420-3433, 2018.
- [30] S. S. Andrews, "Accurate particle-based simulation of adsorption, desorption and partial transmission," *Phys Biol*, vol. 6, no. 4, p. 046015, Nov 12 2009, doi: 10.1088/1478-3975/6/4/046015.



Muneer M. Al-Zubi received his Ph.D. degree in Engineering from the University of Technology Sydney (UTS), Australia, in 2020.

He was an Electronic Circuits Design Engineer with ECE Company, Jordan, from 2010 to 2014. He was with the Jordan University of Science and Technology (JUST), Jordan, from 2014 to 2015, as a Research Assistant and with JODDB, Jordan, from 2015 to 2016, as an Embedded System Design Engineer. From 2017 to 2019, he was a Casual

Academic Lecturer and Research Assistant with the UTS. He worked as a Research Associate at the Center of Excellence for Innovative Projects, JUST, from 2020 to 2021. He is currently a Postdoctoral Researcher with the Department of Engineering, University of Luxembourg, Luxembourg.

Dr. Al-Zubi was ranked first in the class with first-class honors in both MSc and BSc degrees. He was a recipient of various international and local prestigious scholarships. His research interests lie in the areas of Molecular & wireless communication, image processing, and modelling of smart drug delivery systems.



Ananda M. Sanagavarapu received the Ph.D. degree from the Indian Institute of Technology Kharagpur, India.

He was an Associate Professor at the School of Biomedical Engineering, University of Technology Sydney (UTS), Australia.

Prof. Sanagavarapu is a founding core member of the Interdisciplinary Research Centre on Health Technologies, UTS. He received a number of competitive research grants from various Australian Research Councils and industry. He was a co-

recipient of the Priestly Memorial Award from the Institute of Radio and Electronic Engineers, Australia. He was a member of the IEEE in New South Wales Section Committee and was the Past Chair of IEEE NSW AP/MTT joint chapter and was a past Committee Member of IEEE NSW Communications and Signal Processing Society chapter. His current research interests include molecular communications, wireless biomedical communications, implantable biomedical devices, RF and microwave thermal therapies, and microwave imaging.



Peter Plapper received the Ph.D. degree from the RWTH Aachen University, Germany.

For 16 years, he worked in the European and American automotive industry in different positions in Manufacturing Engineering (ME). Since 2010 he is a Full-Professor at the Department of Engineering, University of Luxembourg, Luxembourg.

Prof. Plapper was a recipient of the Borchers Medal of the RWTH Aachen. He is the author of several scientific publications and conference proceedings, editor of four books, and serves as a reviewer of

different research programs. His research interests include digital technologies, industry 4.0, and digitalization of manufacturing processes.



Steve S.H. Ling received the Ph.D. degree from the Department of Electronic and Information Engineering, the Hong Kong Polytechnic University, in 2007.

Currently, he works at the University of Technology Sydney, Australia as a Senior Lecturer.

He has authored and coauthored over 200 books, international journal, and conference papers on Artificial Intelligence and its industrial applications. His current research interests include deep learning in medical imaging, brain-computer interface, and

AI-based biomedical applications. Currently, he serves as Associate Editor for IET Electronics Letters and Sensors.